Cell

Dendrite Self-Avoidance Is Controlled by *Dscam*

Benjamin J. Matthews,[1] Michelle E. Kim,[2,5] John J. Flanagan,[3,5] Daisuke Hattori,[3] James C. Clemens,[4] S. Lawrence Zipursky,[3,*] and Wesley B. Grueber[1,2,*]
[1] Center for Neurobiology and Behavior
[2] Department of Physiology and Cellular Biophysics
Columbia University, 630 W. 168th Street, P&S 11-451, New York, NY 10032, USA
[3] Howard Hughes Medical Institute, Department of Biological Chemistry, David Geffen School of Medicine, University of California, Los Angeles, CA 90095, USA
[4] Department of Biochemistry, Purdue University, 175 S. University, West Lafayette, IN 47907, USA
[5] These authors contributed equally to this work.
*Correspondence: lzipursky@mednet.ucla.edu (S.L.Z.), wg2135@columbia.edu (W.B.G.)
DOI 10.1016/j.cell.2007.04.013

SUMMARY

Dendrites distinguish between sister branches and those of other cells. Self-recognition can often lead to repulsion, a process termed "self-avoidance." Here we demonstrate that dendrite self-avoidance in *Drosophila* da sensory neurons requires cell-recognition molecules encoded by the *Dscam* locus. By alternative splicing, *Dscam* encodes a vast number of cell-surface proteins of the immunoglobulin superfamily. We demonstrate that interactions between identical Dscam isoforms on the cell surface underlie self-recognition, while the cytoplasmic tail converts this recognition to dendrite repulsion. Sister dendrites expressing the same isoforms engage in homophilic repulsion. By contrast, Dscam diversity ensures that inappropriate repulsive interactions between dendrites sharing the same receptive field do not occur. The selectivity of Dscam-mediated cell interactions is likely to be widely important in the developing fly nervous system, where processes of cells must distinguish between self and nonself during the construction of neural circuits.

INTRODUCTION

Dendrites act as information-integrating centers of neurons, and to fulfill this role they must effectively sample sensory or synaptic input. In doing so, some dendrites establish complete and nonredundant territory coverage by following the organizing principles of self-avoidance and tiling. Self-avoidance refers to the tendency for arbors from the same neuron (isoneuronal or sister arbors) to avoid crossing, thereby spreading evenly over a territory (Kramer and Kuwada, 1983). Tiling, by contrast, refers to the complete but nonoverlapping coverage of input space by dendrites from different, but usually functionally related, neurons. Self-avoidance and tiling have so far been identified in many different neuronal systems in both vertebrates and invertebrates (Amthor and Oyster, 1995; Grueber et al., 2002; Grueber and Truman, 1999; Montague and Friedlander, 1991; Sdrulla and Linden, 2006; Sweeney et al., 2002); however, molecular explanations for these phenomena are lacking.

Dendrite self-avoidance and tiling contribute to the patterning of dendritic arborization (da) sensory neurons in the *Drosophila* peripheral nervous system (PNS). The da neurons comprise four morphologically distinct classes (classes I–IV in order of increasing arbor complexity) with dendrites projecting across the epidermis (Grueber et al., 2002). At least three rules appear to govern the organization of these dendritic fields. First, sister dendrites of all da neurons exhibit self-avoidance. Second, the arbors of cells in different classes overlap extensively, providing redundant body wall coverage. Third, the dendrites of adjacent class III and class IV neurons engage in tiling. Repulsive dendrite-dendrite interactions underlie both self-avoidance between sister dendrites and tiling between the dendrites of neighboring neurons of the same class (Grueber et al., 2003b; Sugimura et al., 2003). These multiple levels of interaction between da neuron dendrites create a complex problem in cell recognition. The molecular cues that govern these interactions must promote selective recognition and repulsion between sister dendrites and between dendrites of discrete sets of da neurons while allowing overlap between the dendrites of other cells.

Several studies support the view that *Drosophila* Down syndrome cell-adhesion molecule (Dscam) promotes selective recognition between neurites in the central nervous system (CNS). Dscam is a transmembrane protein comprising extracellular immunoglobulin (Ig) domains and fibronectin type III (FnIII) repeats (Schmucker et al., 2000). Alternative splicing of *Dscam* pre-mRNA potentially

generates 38,016 distinct protein isoforms. These include 19,008 extracellular domains linked to one of two alternative membrane-spanning segments (Schmucker et al., 2000). Biochemical assays have shown that identical ectodomains bind to one another (homophilic binding) with little or no binding to the ectodomains of other isoforms (Wojtowicz et al., 2004). Individual neurons express different combinations of isoforms with few, if any, isoforms shared with neighboring neurons (Neves et al., 2004; Zhan et al., 2004). Dscam molecular diversity might thereby provide a mechanism for distinguishing between self and nonself in neurons (Neves et al., 2004; Zipursky et al., 2006). Mutant studies indicate that *Dscam* is required for axon guidance and targeting, segregation of axon branches, and dendritic patterning in the *Drosophila* CNS (Chen et al., 2006; Hummel et al., 2003; Schmucker et al., 2000; Wang et al., 2002; Zhu et al., 2006). One interpretation of these mutant phenotypes—in particular the failure of sister axons in mushroom body (MB) neurons to diverge and the tight clumping of dendritic arbors of olfactory projection neurons—is that they reflect a defect in neuronal self-recognition and repulsion (Wang et al., 2002; Zhan et al., 2004; Wojtowicz et al., 2004; Zhu et al., 2006; Zipursky et al., 2006). Due to the limited resolution of individual dendritic arbors in the developing CNS, it has not been possible to distinguish between a role for Dscam in cell recognition followed by repulsion or other processes such as neurite outgrowth.

In this study, we explore the role of Dscam in dendrite self-avoidance in the PNS, where it is possible to study interactions between individual dendrites. We find that Dscam is critical for self-avoidance in da neurons and that it is both necessary and sufficient to promote dendrite repulsion where it is expressed. We find that Dscam is dispensable for tiling between cells of the same class, underscoring a primary role in regulating interactions between isoneuronal dendrites. We further show that Dscam mediates self-avoidance through ectodomain-dependent recognition and cytoplasmic domain-dependent repulsion. Dscam molecular diversity ensures that branches from the same neuron selectively recognize and repel only each other, and this specificity is likely crucial for proper elaboration of receptive fields during circuit assembly.

RESULTS

Dscam Is Required for Self-Avoidance in Class I da Neurons

Drosophila da neurons project dendrites across the body wall in a two-dimensional arrangement. Fifteen identified da neurons per abdominal hemisegment comprise four distinct morphological classes (classes I–IV, in order of increasing branching complexity; Figure 1A; Grueber et al., 2002). The dendrites of different da neurons overlap, whereas sister dendrites do not. To assess whether *Dscam* might function in the development of da neurons, we examined expression in the larval PNS. Dscam was detected on the cell bodies, dendrites, and axons of da neurons in second and third instar larvae (Figures 1B and S1A). We did not observe labeling in processes of comparably staged *Dscam* mutant animals (Figures 1C and S1B), indicating that this staining is specific. Furthermore, expression of *UAS-mCD8-GFP* driven by a 5.9 kb fragment of the endogenous *Dscam* promoter fused to *Gal4* (*Dscam-Gal4*) was observed in all da neurons (Figure 1D).

We examined the phenotypic consequences of *Dscam* mutations in class I neurons using $Gal4^{221}$ driving *UAS-mCD8-GFP* as a marker. In second and third instar larvae, these neurons typically extended a simple arbor, with a single primary branch projecting dorsally and secondary and tertiary branches projecting along the anterior-posterior body axis (Figure 1E). These processes exhibited self-avoidance, crossing each other only rarely (Figures 1E and 1G; median [M] = 0 [$0_{Quartile1} - 1_{Quartile3}$] overlaps for ddaD, n = 19; M = 1 [0–1] overlaps for ddaE, n = 18; see Experimental Procedures for details of analysis). By contrast, in *Dscam* mutant embryos and heteroallelic mutant larvae ($Dscam^{21}/Dscam^{23}$; both strong loss-of-function alleles), class I dendrites from the same cell overlapped extensively and fasciculated (Figures 1F–1G and S1D; M = 11.5 [8.25–16] overlaps for ddaD, n = 18; M = 13.5 [10–16.25] overlaps for ddaE, n = 20). Arbors of each cell projected to the same general location but left significant gaps in territory coverage. Live imaging analysis indicated that adhesion between da neurons and their epidermal substrate was not obviously disrupted (data not shown), supporting the conclusion that sister dendrites lacking *Dscam* fail to repel each other when they meet and that this defect leads to crossing and fasciculation of branches.

Dscam is a transmembrane molecule comprising an ectodomain with Ig domains, FnIII repeats, and a cytoplasmic tail with signaling activity (Schmucker et al., 2000). In the course of characterizing a set of *Dscam* alleles, we identified mutants in which Dscam protein was expressed at normal levels. Two of these, $Dscam^{30}$ and $Dscam^{38}$, harbored point mutations within specific extracellular domains (in the second FnIII domain and the tenth Ig domain, respectively). These mutants exhibited self-avoidance phenotypes similar to protein null alleles (data not shown). A third allele, $Dscam^{47}$, carries an in-frame deletion of exon 18 within the cytoplasmic domain (Figure S2). Notably, significant dendrite crossings were observed in $Dscam^{47/23}$ mutants (Figure 2B; M = 3 [2–6] overlaps, n = 23). This phenotype was more severe than $Dscam^{+/23}$ (Figures 2A–2C; M = 0.5 [0–1.25] overlaps, n = 8) and weaker than $Dscam^{21/23}$ (Figure 1G; $p < 0.001$). $Dscam^{47/47}$ mutant class I neurons showed a modest, but significant, self-avoidance phenotype (Figure 2C; M = 1 [0–2] overlaps, n = 24). These data suggest that both the extracellular and intracellular domains of Dscam are important for self-avoidance.

Dscam Functions in All da Neurons to Promote Self-Avoidance

We next asked whether *Dscam* is required cell autonomously for dendritic self-avoidance in all da neurons by generating single neuron mutant clones using the MARCM

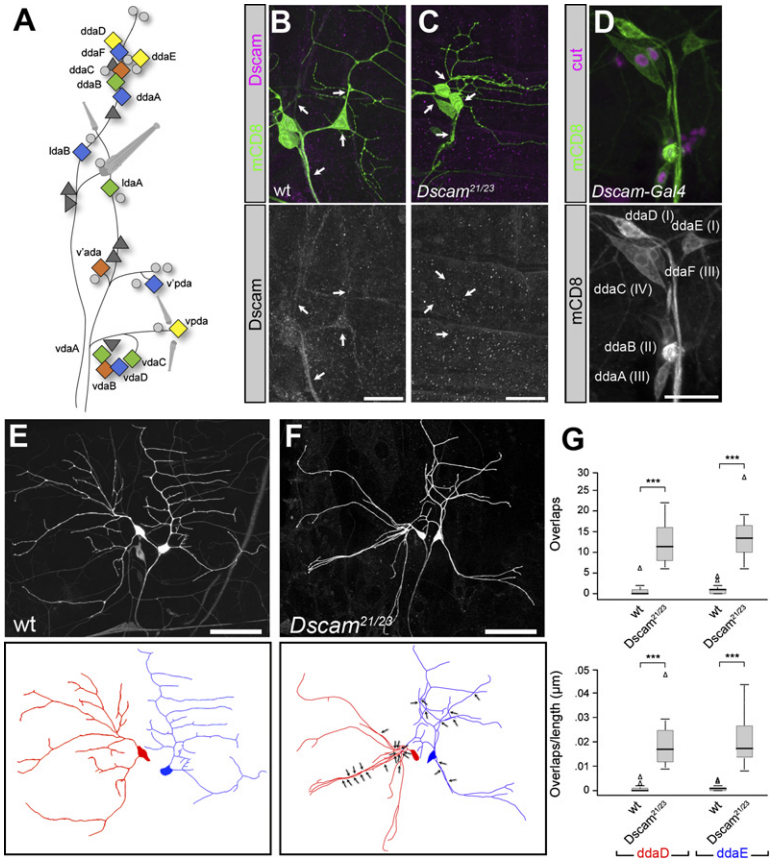

Figure 1. Dscam Expression and Function in da Neurons

(A) Schematic of an abdominal hemisegment of the *Drosophila* larval PNS. Dendritic arborization (da) neurons are indicated by diamonds. Classes are differently colored: class I, yellow; class II, green; class III, blue; class IV, orange. Triangles, other md neurons; circles, external sensory neurons; cylinders, chordotonal organs.

(B) Upper panel: mCD8 driven by $Gal4^{221}$ (green) and Dscam (magenta) immunoreactivity in the dorsal cluster of wild-type larvae. Lower panel: Expression of Dscam. Dscam immunoreactivity was observed in da neuron cell bodies, dendrites, and axons (arrows).

(C) Upper panel: mCD8 driven by $Gal4^{221}$ (green) and Dscam (magenta) immunoreactivity in the dorsal cluster of $Dscam^{21}/Dscam^{23}$ larvae. Lower panel: Dscam staining.

(D) *Dscam-Gal4* drives *UAS-mCD8-GFP* expression in da neurons. Upper panel: Larvae stained for mCD8 (green) and for Cut (magenta) to label the da neurons. Lower panel: Expression of mCD8.

(E) Class I neuron dendrites show self-avoidance. The class IV da neuron ddaC is weakly labeled. ddaD is traced in red and ddaE in blue.

(F) Self-avoidance defects in $Dscam^{21}/Dscam^{23}$ mutant larvae. ddaD is traced in red and ddaE in blue. Dendrite overlaps are indicated by arrows.

(G) Quantification of dendrite overlaps in ddaD and ddaE wild-type and $Dscam^{21}/Dscam^{23}$ animals. n = 19 (wild-type, ddaD); n = 18 (*Dscam,* ddaD); n = 18 (wild-type, ddaE); and n = 20 (*Dscam,* ddaE). Data in boxplot are represented as median (dark line), quartiles Q1–Q3 (25%–75% quantiles; gray box), and data within 1.5× quartile range (dashed bars).

Dorsal is up and anterior to the left in this and all subsequent figures. Genotypes: (B) *FRT42D,* w^+*;* $Gal4^{221}$*, UAS-mCD8-GFP* (C) *FRT42D,* $Dscam^{23}$*/FRT42D,* $Dscam^{21}$*,* $Gal4^{221}$*, UAS-mCD8-GFP* (D) *Dscam-Gal4, UAS-mCD8-GFP*. (E) *FRT42D,* w^+*;* $Gal4^{221}$*, UAS-mCD8-GFP* (F) *FRT42D,* $Dscam^{21}$*/FRT42D,* $Dscam^{23}$*;* $Gal4^{221}$*, UAS-mCD8-GFP*.

Scale bars = 20 μm (B–D); 50 μm (E–F).

system (Lee and Luo, 1999). We examined $Dscam^{23}$ (n = 418), $Dscam^{21}$ (n = 29), and $Dscam^{47}$ (n = 27) clones as well as a control chromosome (n = 181). As was observed in whole-animal preparations, control MARCM clones of class I neurons showed very infrequent dendrite crossings (Figure 3A; *M* = 0 [0–0] overlaps for ddaD, n = 17), whereas dendrites of $Dscam^{23}$ mutant class I neurons overlapped extensively (Figures 3A–3C; *M* = 13 [9–21] overlaps for ddaD, n = 17; total class I, n = 63), with branching and growth unaffected (Figure 3C). Likewise, dendrites in control clones of other da neuron classes crossed only very rarely (Figures 3D, 3F, 3G, and 3I), while dendrites in $Dscam^{23}$ mutant clones of all classes crossed extensively along major dendritic arbors and terminal branches (Figures 3E, 3H, and 3J; n = 32, class II, n = 145, class III, n = 97, class IV). In some instances dendrites collapsed into tangled bundles (e.g., Figure 3H). Targeting was grossly normal in these mutant clones, with two notable exceptions. First, in several clones, main dendritic trunks failed to properly segregate, leaving some regions of the body wall devoid of dendrites (Figure 3B). Second, dendrites in lateral regions of the body wall (from ldaB, ddaA, and ldaA; see Figure 1A) formed dense accumulations near the lateral chordotonal organ (Figure 3H; data not shown; n > 50). Wild-type neurons, by contrast, extended dendrites to the same lateral region of each segment to terminate near the chordotonal organ but arborized more diffusely to cover a larger territory (Figure 3G). Self-avoidance defects of $Dscam^{21}$ single-cell mutant neurons (data not shown) were indistinguishable from $Dscam^{23}$ phenotypes. $Dscam^{47}$ self-avoidance phenotypes were weaker; however, some clones exhibited a notable dendrite collapse phenotype similar to $Dscam^{23}$ neurons (Figures S2E–S2F).

The MARCM clones examined encompassed all da neurons. The phenotypes observed in each clone indicate that *Dscam* provides essential, cell-autonomous control of dendrite self-avoidance.

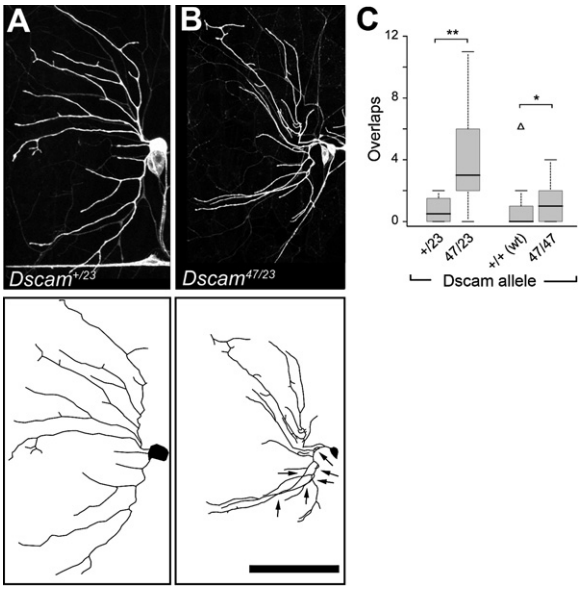

Figure 2. Dscam Cytoplasmic Domain Is Important for Self-Avoidance

(A) Normal self-avoidance in ddaD in *Dscam*$^{+/23}$ heterozygous larvae. (B) Self-avoidance defects in *Dscam*$^{47/23}$ heteroallelic larvae. Arrows indicate overlaps.

(C) Overlaps in (left to right) *Dscam*$^{+/23}$ (n = 8), *Dscam*$^{47/23}$ (n = 23), *Dscam*$^{+/+}$ (wild-type control same as Figure 1G), and *Dscam*$^{47/47}$ (n = 24) ddaD neurons. Data in boxplot are represented as median (dark line), quartiles Q1–Q3 (25%–75% quantiles; gray box), and data within 1.5× quartile range (dashed bars).

Genotypes: (A) *FRT42D, Dscam*^{23}*/FRT42D w*$^{+}$*; Gal4*^{221}*, UAS-mCD8-GFP/+* (B) *FRT42D, Dscam*^{23}*/FRT42D, Dscam*^{47}*; Gal4*^{221}*, UAS-mCD8-GFP.*

Scale bar = 50 μm (A and B).

Intact Tiling between Class IV Neurons in the Absence of Dscam

Given the essential role for Dscam in self-avoidance, we performed a series of experiments to test for a requirement in tiling between da neurons of the same class. Two class IV neurons (v'ada and vdaB) tile the ventral region of the body wall (Grueber et al., 2002). When vdaB neurons were ablated, branches of v'ada invaded the vacated territory and consequently had larger field sizes (Figure 4A and data not shown; n = 5). If recognition and repulsion between these neurons requires *Dscam* function, we predicted that *Dscam* mutant clones would be relieved of growth constraints imposed by surrounding neurons and grow beyond their normal territories. To the contrary, field sizes of wild-type (n = 8) and *Dscam* mutant (n = 5) v'ada MARCM clones were not significantly different (Figure 4A). We verified that dendrites of class IV *Dscam* clones formed boundaries with heteroneuronal dendrites by generating additional MARCM clones in a class-IV-labeled background (using *ppk-eGFP*; Grueber et al., 2003b). *Dscam* mutant clones tiled with adjacent *Dscam* heterozygous neurons (Figure 4B; n = 37 clones), indicating that heteroneuronal recognition and repulsion are not compromised when one cell is mutant for *Dscam*.

We next examined *Dscam* mutant larvae carrying a class IV marker *(ppk-Gal4, UAS-mCD8-GFP)* to determine whether tiling is affected when *Dscam* is removed from neurons on both sides of the tiling boundary. As described above, we observed severe self-avoidance defects within individual class IV neurons; by contrast, the tiling pattern was not obviously disrupted relative to wild-type (Figure 4C, n = 8 wild-type animals, 15–20 cells/animal; Figure 4D, n = 4 mutant animals, 15–20 cells/animal). We combined *Gal4*$^{109(2)80}$ with a FLP-out cassette (Basler and Struhl, 1994; Wong et al., 2002) to differentially label adjacent mutant neurons with CD2 and mCD8-GFP. This labeling strategy allowed mosaic two-color resolution of boundary regions. This analysis indicated that where heteroneuronal mutant terminal branches met, they either stopped, turned, or fasciculated for a short distance (up to approximately 20 μm; Figure 4E, n = 9 cell pairs). Thus, *Dscam* mutant arbors did not invade neighboring territories, and tiling among class IV neurons remained intact.

Together, these results underscore an essential role for *Dscam* in regulating interactions between isoneuronal da neuron dendrites. Given these data, we next wished to examine the role for Dscam diversity in determining the specificity of dendrite-dendrite recognition and the mechanism by which this recognition leads to repulsion.

Single Dscam Isoforms Are Sufficient to Support Cell Recognition and Dendrite Self-Avoidance

The ability of dendrites to distinguish between self and nonself might arise because sister branches present identical Dscam isoforms, while heteroneuronal branches present at least partially distinct sets of isoforms (Neves et al., 2004; Wojtowicz et al., 2004; Zhan et al., 2004). One prediction of this scenario is that individual isoforms would support both self-recognition and dendrite self-avoidance. We tested this possibility in vitro and in vivo.

To assess whether Dscam molecules expressed on cell surfaces support recognition and adhesion, we expressed inducible FLAG-tagged Dscam (either Dscam$^{1.30.30.2}$ or Dscam$^{7.27.25.2}$) in *Drosophila* S2 cells. Uninduced cells, or cells immediately after induction but before substantial levels of Dscam were produced, did not aggregate (Figures 5A and S3). By contrast, induced cells produced substantial levels of Dscam after 6 hr and by this time formed large aggregates (Figures 5B and S3). Thus, similar to findings with purified ectodomains on beads (Wojtowicz et al., 2004), Dscam can mediate recognition between cell surfaces.

To test whether Dscam-mediated aggregation is isoform specific, we mixed two different populations of cells: one population coexpressing Dscam$^{7.27.25.2}$ and RFP and the other coexpressing Dscam$^{7.27.25.2}$ and GFP. Robust aggregation occurred, and all aggregates consisted of green and red cells (Figures 5C and S3; n = 53 aggregates). Importantly, when cells expressing RFP and

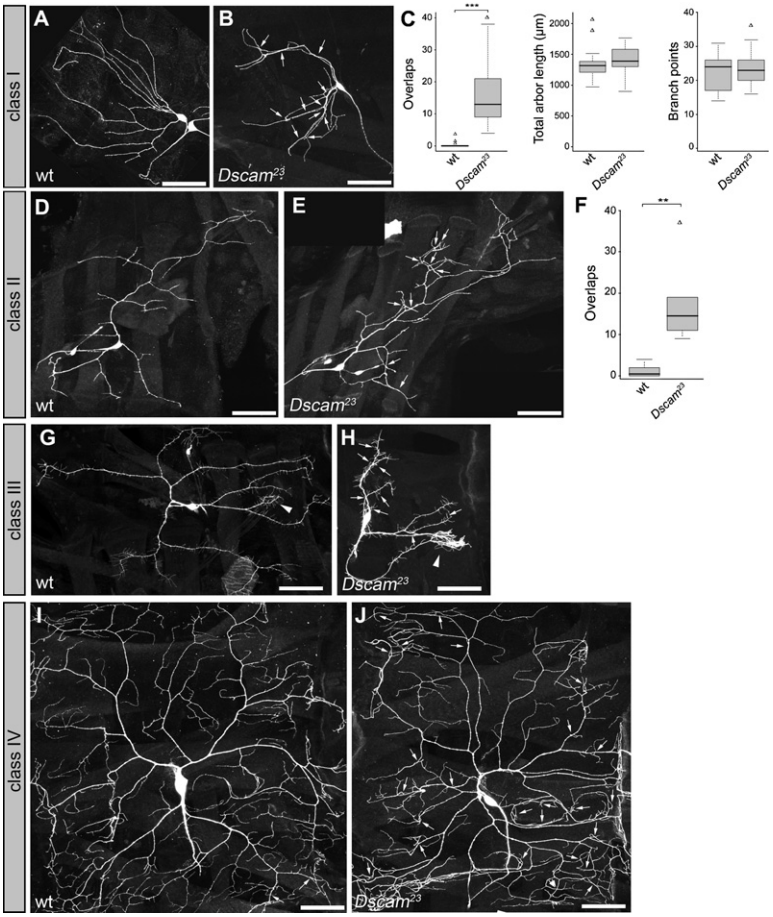

Figure 3. *Dscam* Is Required Cell Autonomously for Self-Avoidance in All da Neurons

(A–C) Class I neurons. (A) Wild-type MARCM clone of ddaD shows normal branch self-avoidance. (B) *Dscam*^{23} clone of ddaD shows extensive overlap and fasciculation of branches (arrows). (C) Quantification of dendrite overlap, length, and branch points in ddaD in wild-type (n = 17) and *Dscam* clones (n = 17).

(D–F) Class II neurons. (D) Wild-type ldaA dendrites do not overlap. (E) *Dscam* ldaA clone shows dendrite overlaps (arrows). (F) Quantification of dendritic overlaps in ldaA neurons. n = 10 (wild-type); n = 6 (*Dscam*).

(G and H) Class III neurons. (G) Wild-type ddaA shows normal self-avoidance with some dendrite branches terminating near the lateral chordotonal organ (arrowhead). (H) *Dscam* ddaA clone shows dendrite overlap (arrows) and collapsed terminal branches at the chordotonal organ (arrowhead).

(I and J) Class IV neurons. (I) Wild-type ddaC neuron shows self-avoidance and occasional dendrite overlaps (arrows). (J) *Dscam* mutant ddaC neuron shows extensive dendrite crossing (arrows).

Data in boxplot are represented as median (dark line), quartiles Q1–Q3 (25%–75% quantiles; gray box), and data within 1.5× quartile range (dashed bars).

Clone genotypes: (A, D, G, and I) *hsFLP, C155-Gal4, UAS-mCD8-GFP/+; FRT42D, w*$^{+}$ (B, E, H, and J) *hsFLP, C155-Gal4, UAS-mCD8-GFP/+; FRT42D, Dscam*^{23}.

Scale bars = 50 μm.

Dscam$^{7.27.25.2}$ were mixed with cells expressing GFP and isoforms differing by only 7, 9, or 11 amino acids in Ig7, mixtures segregated into single-color aggregates consisting entirely of cells expressing the same isoform (Figures 5D and S3; n = 221 aggregates). These data support the view that cell surfaces expressing the same isoforms of Dscam are capable of selective interaction in vitro and indicate that the molecular diversity of Dscam can impart specificity to cell-cell interactions.

Given the ability of individual Dscam isoforms to mediate cell recognition, we asked whether they are also sufficient to support self-avoidance. We first tested the requirement for any specific Dscam isoform for self-avoidance in class I neurons. Self-avoidance defects were pronounced upon removal of all Dscam isoforms (Figures 1G and 5F); however, self-avoidance was not affected by a series of three deletion alleles that removed 3, 5, and 9 of the 12 alternative versions of exon 4 from genomic sequences (Wang et al., 2004a; T. Hummel, M.L. Vasconcelos, J.C.C., and S.L.Z., unpublished data; Figure 5G, *M* = 0 [0–1]; 0 [0–1.25]; and 0 [0–1] overlaps respectively; n = 70). Between these three deletion alleles, every possible exon 4 is deleted, and thus each of the 38,016 possible Dscam isoforms is deleted as well. These data indicate that full Dscam ectodomain diversity is not required for self-avoidance and that no particular isoform is indispensable for avoidance behavior in class I dendrites.

We next examined whether individual Dscam isoforms can rescue *Dscam* loss-of-function phenotypes. Either of two isoforms, Dscam$^{1.30.30.1}$ or Dscam$^{1.30.30.2}$, expressed in a *Dscam* mutant background using *Gal4*^{221} partially, but significantly, rescued the loss-of-function dendrite crossing phenotype in class I neurons (Figures 5H–5I; *M* = 0 [0–1] overlaps for wild-type, n = 23; *M* = 10 [8.75–13.25] overlaps for *Dscam*, n = 20; *M* = 3 [2–4] overlaps for Dscam$^{1.30.30.1}$, n = 17; *M* = 4 [2–4.5] overlaps for Dscam$^{1.30.30.2}$, n = 15). A Dscam isoform with an unrelated ectodomain (Dscam$^{3.36.25.1}$) driven by a 4.5 kb *Dscam* promoter region (Wang et al., 2004a) significantly rescued self-avoidance defects of Dscam mutant class I neurons (Figures 5I and 5J; *M* = 0.5 [0–2] overlaps, n = 12). Whereas Dscam$^{3.36.25.1}$ fully supported self-avoidance, Dscam$^{3.36.25.2}$ expressed under the control of the same promoter did not significantly rescue dendrite overlaps (Figures 5H–5I; *M* = 9 [8–11] overlaps, n = 17; two separate insertions were examined for each promoter-driven isoform and gave indistinguishable results). These data are consistent with previous observations that TM1-containing isoforms preferentially target to dendrites and TM2 isoforms to axons (Wang et al., 2004a; Zhan et al.,

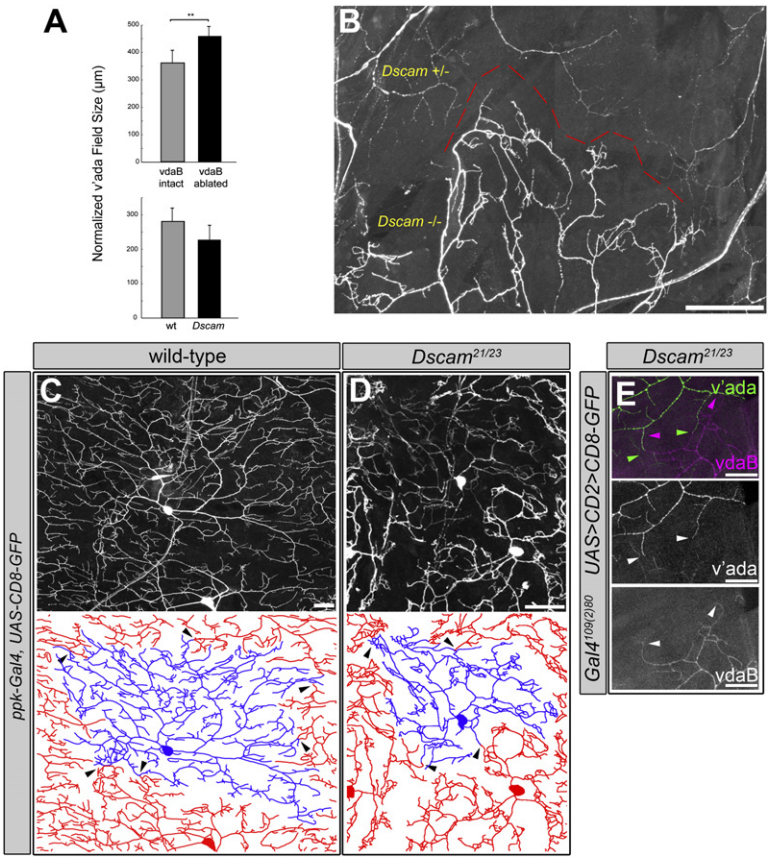

Figure 4. Normal Tiling in *Dscam* Mutant da Neurons

(A) v'ada territory size increases upon neighboring cell ablation but does not increase in *Dscam* mutant clones. Ablations: n = 7 (nonablated); n = 5 (ablated). Clones: n = 8 (wild-type); n = 5 (*Dscam*). Normalized to segment length.

(B) *Dscam*^{23} (*Dscam*$^{-/-}$) mutant vdaB clone generated in a *ppk-eGFP* background. Dscam mutant and adjacent *Dscam*$^{+/23}$ (*Dscam*$^{+/-}$) heterozygous neurons establish normal boundaries (dashed line). n = 37 class IV clones.

(C) Tiling between *ppk-Gal4, UAS-mCD8-GFP*-labeled class IV neurons in wild-type larvae. In (C) and (D) v'ada is traced in blue and surrounding neurons (vdaB, v'ada, and ddaC) in red. Dendrites meet at some boundaries (black arrowheads). Axons are not traced.

(D) Class IV neurons in *Dscam* mutant larvae show self-avoidance defects but intact tiling. Dendrites meet at some boundaries (black arrowheads).

(E) In cases where heteroneuronal arbors meet, FLP-out analysis reveals that dendrites from two mutant cells tile or fasciculate for short distances (arrowheads). n = 9 cell borders were examined.

Genotypes: (B) *hsFLP, C155-Gal4, UAS-mCD8-GFP/+; FRT42D, Dscam*^{23}*; ppk-eGFP/+* (C) *FRT42D, w*$^{+}$*; ppk-Gal4, UAS-mCD8-GFP* (D) *FRT42D, Dscam*^{21}*/ FRT42D, Dscam*^{23}*; ppk-Gal4, UAS-mCD8-GFP* (E) *hsFLP/+; FRT42D, Dscam*^{21}*/ Gal4*$^{109(2)80}$*, FRT42D, Dscam*^{23}*; UAS>CD2>mCD8-GFP/+.*

Data are represented as mean ± SD.

Scale bars = 20 µm.

2004). Higher levels of Gal4-induced expression, however, lead to the accumulation of substantial levels of TM2-containing isoforms also in dendrites (Wang et al., 2004a; Zhan et al., 2004; Figure S4).

Together, these results indicate that single Dscam isoforms are sufficient to mediate recognition between cell surfaces and to initiate self-avoidance of dendrites and that the identity of the ectodomain is unimportant for these activities.

Misexpression of Single Isoforms in Different Cells Promotes Heteroneuronal Dendrite Avoidance

The dendrites of different da neurons normally overlap. The finding that single isoforms can support self-avoidance suggests that Dscam diversity between different cells might be required for them to pattern their dendrites without mutual repulsion. To test this, we forced wild-type neurons with normally overlapping dendrites to express the same predominant Dscam isoform. We focused our analysis on a class I neuron (vpda) and a class III neuron (v'pda). In third instar larvae, these arbors showed extensive overlap of both main dendritic trunks and fine terminal branches (Figures 6A and 6D; *M* = 13 [12–15] overlaps, n = 34 cell pairs). Likewise, when a single Dscam isoform, Dscam$^{1.30.30.1}$, was expressed highly in the class I neuron using the *Gal4*^{221} driver, class I dendrites showed considerable overlap with class III branches (Figures 6D and S4; *M* = 7 [6–9] overlaps, n = 27). In contrast, when Dscam was expressed in both cells using the pan-da neuron driver *Gal4*$^{109(2)80}$, very few overlaps occurred between them, and their arbors became segregated (Figures 6B–6D; *M* = 1 [0–2.5] overlaps for Dscam$^{1.30.30.1}$, n = 23; *M* = 1 [0–3] overlaps for Dscam$^{11.31.25.1}$, n = 28). Ectopic avoidance occurred irrespective of ectodomain identity (Figure 6D), and isoforms containing the TM2 domain also produced repulsion when driven at high levels by *Gal4*$^{109(2)80}$ (Figures 6D and S4; *M* = 2 [0–3] overlaps for Dscam$^{1.30.30.2}$, n = 31; *M* = 2 [1–4] overlaps for Dscam$^{11.31.25.2}$, n = 51). Expression of epitope-tagged versions of Dscam, Dscam$^{1.30.30.1\text{-Flag}}$ and Dscam$^{1.30.30.2\text{-Flag}}$, induced ectopic avoidance and these isoforms localized along the dendritic arbors of both class I and class III neurons (Figure S4).

These data indicate that if different da neurons express the same predominant Dscam isoforms, they are prevented from forming overlapping fields. These studies therefore demonstrate that Dscam diversity is crucial for appropriate patterning of ensembles of dendrites.

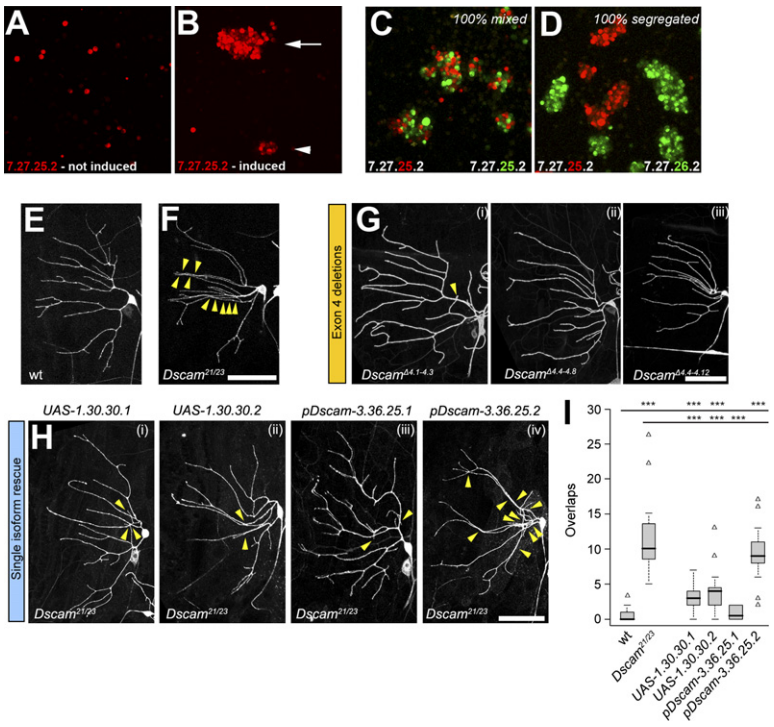

Figure 5. Single Dscam Isoforms Support Cell-Surface Recognition and Self-Avoidance

(A) RFP-labeled S2 cells after six hours of aggregation without induction of Dscam expression.

(B) RFP-labeled induced cells expressing Dscam$^{7.27.25.2}$. Aggregates of greater than ten cells were included in tally (arrow). Aggregates of less than ten cells were not included in tally (arrowhead).

(C) Images of results from mixing of an RFP- and a GFP-labeled population of S2 cells each transfected with the same Dscam isoform.

(D) Images of results from mixing of an RFP- and a GFP-labeled population of S2 cells each transfected with highly similar, but nonidentical, Dscam isoforms.

(E) Wild-type class I neuron ddaD. In (E)–(H) the class I neuron ddaD is visualized using *Gal4^{221}, UAS-mCD8-GFP.*

(F) ddaD self-avoidance phenotype in *Dscam$^{21/23}$* larvae. Arrowheads indicate dendrite crossings.

(G) Dorsal class I neuron ddaD from (i) *Dscam$^{\Delta 4.1\text{-}4.3}$* (n = 22), (ii) *Dscam$^{\Delta 4.4\text{-}4.8}$* (n = 24), and (iii) *Dscam$^{\Delta 4.4\text{-}4.12}$* (n = 24) larvae. Arrowhead indicates dendrite crossing.

(H) Dorsal class I neuron ddaD in *Dscam$^{21/23}$* larvae expressing (i) *UAS-Dscam$^{1.30.30.1}$* or (ii) *UAS-Dscam$^{1.30.30.2}$* via *Gal4^{221}* or expressing (iii) *Dscam$^{3.36.25.1}$* or (iv) *Dscam$^{3.36.25.2}$* via a *Dscam* promoter (*pDscam)*. Arrowheads indicate dendrite crossings.

(I) Quantification of overlaps from rescue experiments. n = 23 (wild-type); n = 20 (*Dscam$^{21/23}$*); n = 17 (*UAS-Dscam$^{1.30.30.1}$*); n = 15 (*UAS-Dscam$^{1.30.30.2}$*); n = 12 (*pDscam-Dscam$^{3.36.25.1}$*); and n = 17 (*pDscam-Dscam$^{3.36.25.2}$*). Data in boxplot are represented as median (dark line), quartiles Q1–Q3 (25%–75% quantiles; gray box), and data within 1.5× quartile range (dashed bars).

Genotypes: (E) *FRT42D, w^{+}; Gal4^{221}, UAS-mCD8-GFP/+* (F) *FRT42D, Dscam^{21}/FRT42D, Dscam^{23}; Gal4^{221}, UAS-mCD8-GFP/+* (G) (i) *FRTG13, Dscam$^{\Delta 4.1\text{-}4.3}$; Gal4^{221}, UAS-mCD8-GFP* (ii) *Dscam$^{\Delta 4.4\text{-}4.8}$; Gal4^{221}, UAS-mCD8-GFP* (iii) *Dscam$^{\Delta 4.4\text{-}4.12}$; Gal4^{221}, UAS-mCD8-GFP* (H) (i) *FRT42D, Dscam^{21}/FRT42D, Dscam^{23}; Gal4^{221}, UAS-mCD8-GFP/UAS-Dscam$^{1.30.30.1}$*, (ii) *FRT42D, Dscam^{21}/FRT42D, Dscam^{23}; Gal4^{221}, UAS-mCD8-GFP/UAS-Dscam$^{1.30.30.2}$*, (iii) *FRT42D, Dscam^{21}/FRT42D, Dscam^{23}; Gal4^{221}, UAS-mCD8-GFP/pDscam-Dscam$^{3.36.25.1}$*, (iv) *FRT42D, Dscam^{21}/FRT42D, Dscam^{23}; Gal4^{221}, UAS-mCD8-GFP/pDscam-Dscam$^{3.36.25.2}$*.

Scale bars = 50 μm.

The Cytoplasmic Domain Converts Branch Recognition to Repulsion

How do adhesive interactions between Dscam ectodomains, such as those observed in S2 cells (Figure 5) or between Dscam-decorated beads and cells (Wojtowicz et al., 2004), give rise to the repulsive responses in da neuron dendrites described in this study? To address this apparent paradox, we tested the role of the cytoplasmic domain in the conversion of homophilic interactions into repulsive signaling. Whereas expression of a Dscam isoform with a deleted cytoplasmic tail (Dscam$^{1.30.30.1\text{-}\Delta C\text{-}GFP}$; Zhu et al., 2006) was sufficient to induce aggregation between cells in vitro (data not shown), this truncated Dscam failed to rescue the *Dscam* mutant phenotype in class I da neurons (Figure S5; n = 27). These data suggest that the difference between adhesion and repulsion in these different cellular contexts lies in the cytoplasmic tail.

Cell-surface association may correspond to an intermediate step of Dscam self-avoidance activity. To examine whether associations are made between dendrites expressing Dscam isoforms with compromised signaling, we expressed Dscam$^{1.30.30.1\text{-}\Delta C\text{-}GFP}$ under the control of *Gal4$^{109(2)80}$*. Unlike the segregation of fields observed with full-length Dscam expression (Figures 6B–6D), class I and III arbors, both expressing Dscam$^{1.30.30.1\text{-}\Delta C\text{-}GFP}$, overlapped and formed numerous branch-to-branch complexes and fasciculated bundles (Figures 7A and 7B; n = 26 cell pairs and 1214 ends). To determine whether the dendrite bridges between heteroneuronal dendrites were stable or transient, we performed time-lapse studies. Live imaging of larvae expressing Dscam$^{1.30.30.1\text{-}\Delta C\text{-}GFP}$ under the control of *Gal4$^{109(2)80}$* revealed that these dendrites were able to grow along each other and that dendrite tips often formed persistent contacts or bridges to dendritic shafts (Figure 7C; Movie S1, n = 5 animals). This behavior was in contrast to neurons expressing full-length Dscam$^{1.30.30.1}$, where stable bridges and fasciculation were not observed (Movie S2, n = 9 animals). These data suggest a functional separation of recognition and repulsion activity in Dscam-mediated self-avoidance. The ectodomain of Dscam initiates self-avoidance through

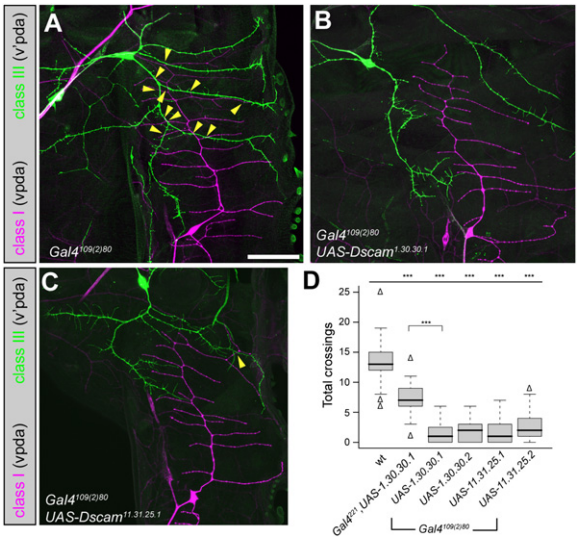

Figure 6. Normally Overlapping Dendritic Fields Segregate upon Overexpression of Single Dscam Isoforms

(A) Wild-type pattern of dendrites of class I (vpda, magenta) and class III (v'pda, green). Neurons are differentially labeled using a FLP-out cassette together with the pan-da neuron driver *Gal4*$^{109(2)80}$. These class I and class III arbors normally overlap (arrowheads).

(B) Overexpression of Dscam$^{1.30.30.1}$ using *Gal4*$^{109(2)80}$ causes class I (magenta) and class III (green) arbors to segregate into nonoverlapping territories.

(C) Overexpression of Dscam$^{11.31.25.1}$ using *Gal4*$^{109(2)80}$ causes class I (magenta) and class III (green) arbors to segregate.

(D) Quantification of dendrite crossings between class I (vpda) and class III (v'pda) arbor pairs. *Gal4*^{221} drives expression strongly in the class I neuron vpda, and *Gal4*$^{109(2)80}$ drives in all da neurons. n = 34 (wild-type); n = 27 (*Gal4*^{221}, *UAS-Dscam*$^{1.30.30.1}$); n = 23 (*Gal4*$^{109(2)80}$, *UAS-Dscam*$^{1.30.30.1}$); n = 31 (*Gal4*$^{109(2)80}$, *UAS-Dscam*$^{1.30.30.2}$); n = 28 (*Gal4*$^{109(2)80}$, *UAS-Dscam*$^{11.31.25.1}$); and n = 51 (*Gal4*$^{109(2)80}$, *UAS-Dscam*$^{11.31.25.2}$). Data in boxplot are represented as median (dark line), quartiles Q1–Q3 (25%–75% quantiles; gray box), and data within 1.5× quartile range (dashed bars).

Genotypes: (A) *hsFLP/+; Gal4*$^{109(2)80}$*/+; UAS>CD2>mCD8-GFP/+* (B) *hsFLP/+; Gal4*$^{109(2)80}$*/+; UAS>CD2>mCD8-GFP/UAS-Dscam*$^{1.30.30.1}$ (C) *hsFLP/+; Gal4*$^{109(2)80}$*/+; UAS>CD2>mCD8-GFP/UAS-Dscam*$^{11.31.25.1}$.

Scale bars = 50 μm.

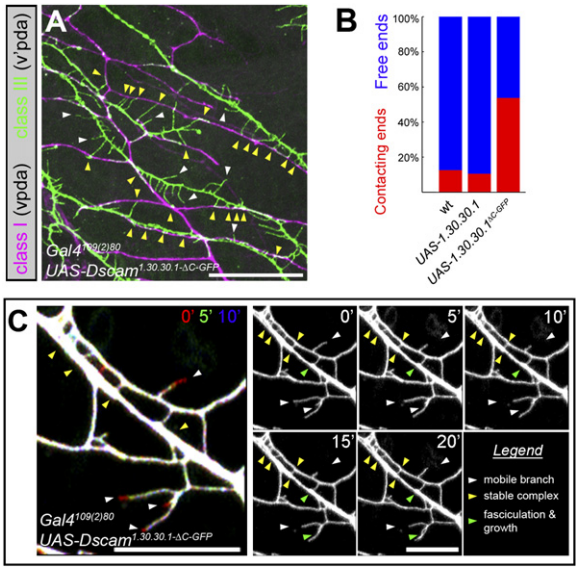

Figure 7. The C-Terminal Domain of Dscam Converts Branch Recognition and Attachment to Repulsion

(A) Class I (magenta) and class III (green) neurons expressing Dscam$^{1.30.30.1\text{-}\Delta C\text{-}GFP}$ and *UAS>CD2>mCD8-GFP* via the da neuron driver *Gal4*$^{109(2)80}$. Dendrite-dendrite bridging and fasciculation are extensive (yellow arrowheads).

(B) Percentage of class III branch tips in contact with dendrites from the class I cell vpda in wild-type, Dscam$^{1.30.30.1}$-overexpressing, and Dscam$^{1.30.30.1\text{-}\Delta C\text{-}GFP}$-overexpressing animals. n = 1346 ends, 20 cell pairs (wild-type); n = 612 ends, 18 cell pairs (*UAS-Dscam*$^{1.30.30.1}$); and n = 1214 ends, 26 cell pairs (*UAS-Dscam*$^{1.30.30.1\text{-}\Delta C\text{-}GFP}$).

(C) In vivo time-lapse imaging of neurons expressing *UAS-Dscam*$^{1.30.30.1\text{-}\Delta C\text{-}GFP}$ and *UAS-mCD8-GFP* via *Gal4*$^{109(2)80}$. Left panel: Red, green, and blue channels are separated by 5 min. For complete series, see Movie S1. Dynamic dendrites not associated with other branches are red, blue, or green (white arrowheads). Dendrites that remain stable are white (yellow arrowheads). Right panel: Individual time points; arrowheads indicate branch behaviors as detailed in legend.

Genotypes: (A) *hsFLP/+; Gal4*$^{109(2)80}$*/+; UAS>CD2>mCD8-GFP/UAS-Dscam*$^{1.30.30.1\text{-}\Delta C\text{-}GFP}$ (C) *Gal4*$^{109(2)80}$*, UAS-mCD8-GFP/+; +/UAS-Dscam*$^{1.30.30.1\text{-}\Delta C\text{-}GFP}$.

Scale bars = 50 μm (A) and 5μm (C).

homophilic recognition and adhesion, while the cytoplasmic tail is required to convert attachment to repulsion between sister branches.

DISCUSSION

Cell-specific repulsive interactions between developing arbors of invertebrate and vertebrate neurons ensure complete and nonoverlapping coverage of receptive territories. This organization is likely essential for proper information processing in the nervous system (Grueber et al., 2003b; Hitchcock, 1989; Kramer and Stent, 1985; Sagasti et al., 2005; Sugimura et al., 2003). The molecular basis of dendrodendritic repulsion underlying self-avoidance has not been determined. Our data show that dendrite self-avoidance in da neurons relies on cell-surface recognition molecules encoded by the *Dscam* locus. We provide strong evidence that Dscam mediates contact-dependent repulsion and that Dscam diversity underlies a robust cellular recognition mechanism allowing dendrites to distinguish between the surfaces of different cells. Based on these findings and previous studies of Dscam's role in wiring the brain, we argue that Dscam-mediated self-avoidance is a general organizing mechanism operating throughout the *Drosophila* nervous system.

Dscam Controls Self-Avoidance

Our data demonstrate a cell-autonomous role for *Dscam* function in self-avoidance in all classes of *Drosophila* da neurons. da neurons associate closely with the epidermis as they extend across the body wall; thus, their dendrites create a two-dimensional meshwork in which developing

branches frequently encounter other dendrites (Bodmer and Jan, 1987). This is in contrast to the layout of the CNS, in which axons and dendrites usually elaborate in three dimensions. By examining da neurons, we were able to analyze the behavior of individual branches within a single dendritic arbor at high resolution. This allowed critical quantitative examination of the mechanisms underlying selective recognition between dendrites. Our data show that when deficient in Dscam function, individual dendrites do not recognize sister branches and fail to initiate repulsion, leading to a breakdown in self-avoidance. Individual branches of *Dscam* mutant cells often failed to evenly disperse across their territory. Additionally, processes from specific da neurons gathered at nonrandom, discrete target sites within their territory (see below).

Dscam is likely to play a similar role in the CNS based on axonal- and dendritic-arborization phenotypes. In the olfactory system, for example, the terminal processes of single mutant olfactory receptor neurons, projection neurons, and interneurons (Hummel et al., 2003; Zhu et al., 2006) form clumps. While this might reflect a phenotype of self-avoidance, the resolution of these studies was not sufficient to distinguish between self-avoidance and other mechanisms such as branch extension and synapse formation. By contrast, single-branch resolution has been achieved for *Dscam* defects in the axonal projections of MB neurons. *Dscam* is required for proper segregation of sister axon branches (Wang et al., 2002), and analogous to the self-avoidance control in da neurons, specific isoforms do not appear to provide instructive cues for this segregation event (Wang et al., 2004a; Zhan et al., 2004). It has been argued that this reflects a role for Dscam in mediating self-recognition and repulsion between these axons (Wang et al., 2002; Wojtowicz et al., 2004; Zhan et al., 2004). In da neurons, dendrite self-avoidance defects were separable from growth, branching, and targeting errors and were fully penetrant. Thus, our data directly implicate *Dscam* in self-avoidance and demonstrate this role at the level of interactions between individual branches.

Dscam-Mediated Cell Recognition Promotes Contact-Dependent Repulsion

The simplest model for a direct role for Dscam in self-recognition is one in which identical Dscam ectodomains on the surfaces of isoneuronal dendrites recognize each other and induce a subsequent repulsive signal that is mediated by domains in the cytoplasmic tail. This model is supported by both in vitro and in vivo data presented in this paper. First, identical Dscam isoforms expressed in two cell populations in vitro induced their aggregation in an isoform-specific manner, showing that Dscam provides cells with the ability to distinguish between different cell surfaces. Second, ectopic expression of identical Dscam isoforms on the dendrites of different cells, which normally overlap, promoted growth away from each other.

How can in vitro adhesion be reconciled with in vivo repulsion? Our data suggest that the dendrites of da neurons convert an initial Dscam-dependent cell-surface interaction into a repulsive response, which leads to dendrite separation and receptive field elaboration. da dendrites expressing a form of Dscam in which the cytoplasmic domain was replaced with GFP formed stable bridges. These data are reminiscent of studies demonstrating that complexes of ephrin-A2 and EphA3 are intermediates in heterophilic repulsive interactions in cell culture (Hattori et al., 2000). Ephrin-A2 is normally cleaved by a metalloprotease, and cleavage-resistant mutations lead to more stable interactions between growth cones and target cells (Hattori et al., 2000).

The signal transduction mechanism promoting repulsion is poorly understood. We show that at least some self-avoidance activity derives from sequences encoded by exon 18 in the Dscam cytoplasmic tail, which includes a polyproline motif. In previous studies, the Dock adaptor protein was shown to bind to this region as well as to other sites on the cytoplasmic domain and to act downstream of Dscam in axon guidance (Schmucker et al., 2000). While Dock has been implicated in the repulsive signaling downstream from the slit receptor, Robo (Fan et al., 2003), loss-of-function Dock mutations caused no obvious self-avoidance defects in da neurons (data not shown). Dock may not function in self-avoidance or, alternatively, it may be redundant with other signaling pathways. The Tricornered (Trc) signaling pathway was previously shown to regulate tiling and self-avoidance in class IV neurons (Emoto et al., 2004); however, examination of animals carrying trans-heterozygous mutant combinations did not uncover a genetic interaction between *trc* and *Dscam* (data not shown).

Importance of Dscam Molecular Diversity for Selective Self-Avoidance in da Neurons

Alternative splicing of *Dscam* pre-mRNA can generate an enormous number of distinct cell-surface receptors (Schmucker et al., 2000). Is Dscam diversity, or any specific Dscam isoform, necessary for self-avoidance in individual da neurons? Our results argue that while diversity is not strictly required for self-recognition and repulsion, it is crucial to prevent inappropriate repulsive interactions from occurring between the dendrites of different cells. This may be a central function for Dscam diversity both in different functional groups of sensory neurons in the PNS, which must sample input from overlapping regions of the body wall, and in regions of the CNS with much more highly intermingled dendritic and axonal processes.

Previous data suggest an analogous function for Dscam diversity in mediating the sorting of axons in the developing MB (Zhan et al., 2004). MB axon phenotypes were partially rescued by expression of single isoforms, whereas ectopic expression across multiple cells gave dominant effects, in which axons were guided to improper targets (Zhan et al., 2004). These data together with studies described here indicate that axons that project along a common fascicle or dendrites with overlapping fields must express sufficiently different isoform repertoires. Supporting this scenario, expression of Dscam isoforms

in MB neurons, as well as photoreceptor subtypes, appears to be specified through a stochastic mechanism whereby each neuron expresses a biased, yet largely nonspecific set of isoforms (Neves et al., 2004; Zhan et al., 2004). Given the complexity of the *Dscam* locus, it is reasonable to expect that different roles for diversity will be observed in different cell populations or even different processes of a cell. For example, our results are not incompatible with Dscam diversity also contributing to wiring in a more deterministic fashion wherein specific isoforms are required for elaborating different aspects of neural circuits (Chen et al., 2006).

Self-Avoidance and Patterning of the Nervous System

Dendritic arbors respond to numerous intrinsic and extrinsic cues during morphogenesis (Jan and Jan, 2003; Miller and Kaplan, 2003; Whitford et al., 2002). How might self-avoidance mechanisms operate in the context of these other patterning events during the assembly of neural circuits? *Dscam* mutant phenotypes in da neurons provide insight into this problem. Mutant isoneuronal dendrites freely overlapped along their length, and the dendrites of some cells collected into tight bundles at stereotyped locations along the body wall. Mutant dendrites rarely grew beyond these specific sites of termination. Interestingly, wild-type dendrites normally projected to these same foci but provided a more diffuse coverage of the surrounding area, very likely because self-avoidance prohibited their overlap. These observations together suggest that *Dscam* mutant phenotypes reveal coordinates on the body wall that are attractive to dendrites and that there is an important interplay in da neurons between self-avoidance signaling and dendrite guidance mechanisms.

One implication of these observations for circuit assembly is that self-avoidance is likely crucial for the spreading of highly branched dendritic processes that might otherwise tend to fasciculate or respond in unison to localized extrinsic guidance signals. In this way, self-avoidance might act throughout the nervous system to establish properly targeted and fully sampled territories. The analogies between *Dscam* mutant phenotypes in the brain and those of da neurons we have described here support this notion (Hummel et al., 2003; Wang et al., 2002; Zhan et al., 2004; Zhu et al., 2006). Based on these findings, we propose that Dscam-mediated self-avoidance plays a widespread role in patterning the fly nervous system. As Dscam diversity is not seen in vertebrate neurons (Crayton et al., 2006), we speculate that analogous mechanisms might exist in which stochastic expression of other families of cell-surface recognition molecules provide the capacity for self-avoidance in the vertebrate brain.

EXPERIMENTAL PROCEDURES

Fly Stocks

For visualizing and manipulating da neurons we used *ppk-eGFP* (Grueber et al., 2003b) and *ppk-Gal4* (Grueber et al., 2007) for class IV neurons, $Gal4^{221}$ (Grueber et al., 2003a) for class I neurons, and $Gal4^{109(2)80}$ (Gao et al., 1999) for all classes. $Dscam^{21}$ *and* $Dscam^{23}$ have been described previously (Hummel et al., 2003). The characterization of the $Dscam^{47}$ mutation is described in Supplemental Experimental Procedures. For mutant analysis, the $Dscam^{21}$ and $Dscam^{23}$ chromosomes were cleaned by crossing to an *FRT42D* w^+ chromosome for five successive rounds of recombination. The *Dscam* deletion mutants removing exons 4.1–4.3 and 4.4–4.12 have been described previously (Wang et al., 2004a). The 4.4–4.8 deletion was generated by *P* element excision by T. Hummel and M.L. Vasconcelos in the lab of S.L.Z. The breakpoints of this line were determined by sequencing. Microarray analysis of 4.4–4.12 flies confirmed expression of isoforms only containing exons 4.1–4.3. The generation of *Dscam-Gal4* and *Dscam* affinity-tagged constructs is described in Supplemental Experimental Procedures. Other mutant alleles used were $Dock^{P1}$ (Garrity et al., 1996) and trc^1 (Geng et al., 2000).

Mosaic Analysis

For MARCM clones we crossed *hsFLP, C155-Gal4, UAS-mCD8-GFP; FRT42D, tubP-Gal80/CyO* to *FRT42D* $Dscam^{21}$*/CyO, FRT42D* $Dscam^{23}$*/CyO,* or *FRT42D* $Dscam^{47}$*/CyO*. Clones were generated as previously described (Grueber et al., 2002). Control clones were made using the *FRT42D* w^+ chromosome used for mutant outcrossing (see above). For Dscam overexpression experiments we crossed *hsFLP;* $Gal4^{109(2)80}$*; UAS>CD2>mCD8-GFP* (Wang et al., 2004b; Wong et al., 2002) to lines carrying *UAS-Dscam* transgenes. For experiments using *UAS>CD2>mCD8-GFP,* brief heat shock at 37.5°C was used to induce mosaic expression of CD2 and mCD8-GFP.

Immunohistochemistry

Immunohistochemistry was performed as previously described (Grueber et al., 2002). See Supplemental Experimental Procedures for details.

Live Imaging

Second or third instar larvae were placed on a slide in a drop of 90% glycerol or a 50% mix of Series 27 and 700 Halocarbon oil, covered with a "0" thickness coverslip, and imaged by confocal microscopy using 63× Plan Neofluar (1.3 N.A.) water/glycerol- or 40× Plan Neofluar (1.3 N.A.) oil-immersion objectives. Animals were imaged for up to 60 min, removed from glycerol, rinsed in PBS, and returned to a grape plate.

Ablations

Ablations were performed using a Micropoint laser system (Photonic Instruments, St. Charles, IL) as described previously (Grueber et al., 2003b).

Aggregation Analysis

S2 cells (3×10^6/5 ml) were transfected with 2 ug of plasmid DNA using Effectene (Qiagen). Cells were pelleted 72 hr posttransfection, resuspended at a concentration of 2×10^6 cells/ml. Cells (1 ml) were transferred to an Eppendorf tube and induced with copper sulfate (0.7 mM) where applicable. Cells were agitated at 150 RPM for 6 hr at room temperature. An aliquot of cells (100 μl of a 1:5 dilution) was spotted into two separate 35 mm glass-bottom microwell dishes (MatTek Corporation), and clusters consisting of more than 10 cells were counted. GFP and RFP markers were visualized on a Zeiss 510 Meta confocal microscope. Additional details can be found in Supplemental Experimental Procedures.

Image Acquisition and Analysis

Images were acquired on a Zeiss 510 Meta confocal microscope using 40× Plan Neofluar 1.3 N.A. and 25× Plan Neofluar 1.4 N.A. lenses. When arbors could not be scanned in a single frame, multiple images of adjacent areas were assembled using Photoshop CS2 (Adobe Systems, San Jose, CA). Dendrites were traced using Neurolucida

(MBF Bioscience, Williston, VT). Quantification was performed with Neurolucida Explorer, custom MATLAB scripts (Mathworks, Natick, MA), and ImageJ (National Institutes of Health, Bethesda, MD). n values indicate number of cells examined, or, where appropriate, cell pairs. Statistical analysis was performed in R (R Development Core Team, 2006). Normality was assessed by the Shapiro-Wilk test, and where data were not normally distributed, statistical differences between data sets were tested by Wilcoxon rank sum. Such data sets are represented in boxplots as median, quartiles Q1–Q3 (25%–75% quantiles), and data in 1.5× quartile range. Data points outside this range are represented as triangles. Values were calculated using R. Student's t test was used for data presented in Figure 4. Data in bar graphs are represented as mean ± SD. All p values are indicated as: * = $p < 0.05$, ** = $p < 0.01$, and *** = $p < 0.001$.

Supplemental Data

Supplemental Data include Experimental Procedures, References, five figures, and two movies and can be found with this article online at http://www.cell.com/cgi/content/full/129/3/593/DC1/.

ACKNOWLEDGMENTS

We are grateful to H. Hing, T. Lee, L. Luo, B. McCabe, G. Struhl, the Bloomington Stock Center, and the Developmental Studies Hybridoma Bank for fly stocks and antibodies and to O. Hobert and R. Poole for assistance with ablations. We thank T. Jessell, J. Dodd, M. Corty, and M. Zlatic for comments on the manuscript. We also thank Dietmar Schmucker and Yuh-Nung Jan for discussions and sharing unpublished results. This is journal paper number 18080 of Purdue University Agricultural Experiment Station (J.C.C.). S.L.Z. is an investigator of the Howard Hughes Medical Institute. This work was supported by start-up funds from Columbia University and a grant from the Gatsby Initiative in Brain Circuitry (W.B.G.).

Received: October 25, 2006
Revised: February 7, 2007
Accepted: April 9, 2007
Published: May 3, 2007

REFERENCES

Amthor, F.R., and Oyster, C.W. (1995). Spatial organization of retinal information about the direction of image motion. Proc. Natl. Acad. Sci. USA *92*, 4002–4005.

Basler, K., and Struhl, G. (1994). Compartment boundaries and the control of Drosophila limb pattern by hedgehog protein. Nature *368*, 208–214.

Bodmer, R., and Jan, Y.N. (1987). Morphological differentiation of the embryonic peripheral neurons in *Drosophila*. Rouxs Arch. Dev. Biol. *196*, 69–77.

Chen, B.E., Kondo, M., Garnier, A., Watson, F.L., Puettmann-Holgado, R., Lamar, D.R., and Schmucker, D. (2006). The molecular diversity of Dscam is functionally required for neuronal wiring specificity in Drosophila. Cell *125*, 607–620.

Crayton, M.E., 3rd, Powell, B.C., Vision, T.J., and Giddings, M.C. (2006). Tracking the evolution of alternatively spliced exons within the Dscam family. BMC Evol. Biol. *6*, 16.

Emoto, K., He, Y., Ye, B., Grueber, W.B., Adler, P.N., Jan, L.Y., and Jan, Y.N. (2004). Control of dendritic branching and tiling by the tricornered-kinase/furry signaling pathway in *Drosophila* sensory neurons. Cell *119*, 245–256.

Fan, X., Labrador, J.P., Hing, H., and Bashaw, G.J. (2003). Slit stimulation recruits Dock and Pak to the roundabout receptor and increases Rac activity to regulate axon repulsion at the CNS midline. Neuron *40*, 113–127.

Gao, F.B., Brenman, J.E., Jan, L.Y., and Jan, Y.N. (1999). Genes regulating dendritic outgrowth, branching, and routing in Drosophila. Genes Dev. *13*, 2549–2561.

Garrity, P.A., Rao, Y., Salecker, I., McGlade, J., Pawson, T., and Zipursky, S.L. (1996). *Drosophila* photoreceptor axon guidance and targeting requires the dreadlocks SH2/SH3 adapter protein. Cell *85*, 639–650.

Geng, W., He, B., Wang, M., and Adler, P.N. (2000). The *tricornered* gene, which is required for the integrity of epidermal cell extensions, encodes the *Drosophila* nuclear DBF2-related kinase. Genetics *156*, 1817–1828.

Grueber, W.B., and Truman, J.W. (1999). Development and organization of a nitric-oxide-sensitive peripheral neural plexus in larvae of the moth, Manduca sexta. J. Comp. Neurol. *404*, 127–141.

Grueber, W.B., Jan, L.Y., and Jan, Y.N. (2002). Tiling of the Drosophila epidermis by multidendritic sensory neurons. Development *129*, 2867–2878.

Grueber, W.B., Jan, L.Y., and Jan, Y.N. (2003a). Different levels of the homeodomain protein cut regulate distinct dendrite branching patterns of Drosophila multidendritic neurons. Cell *112*, 805–818.

Grueber, W.B., Ye, B., Moore, A.W., Jan, L.Y., and Jan, Y.N. (2003b). Dendrites of distinct classes of Drosophila sensory neurons show different capacities for homotypic repulsion. Curr. Biol. *13*, 618–626.

Grueber, W.B., Ye, B., Yang, C.H., Younger, S.H., Borden, K., Jan, L.Y., and Jan, Y.N. (2007). Projections of Drosophila multidendritic neurons in the central nervous system: links with peripheral dendrite morphology. Development *134*, 55–64.

Hattori, M., Osterfield, M., and Flanagan, J.G. (2000). Regulated cleavage of a contact-mediated axon repellent. Science *289*, 1360–1365.

Hitchcock, P.F. (1989). Exclusionary dendritic interactions in the retina of the goldfish. Development *106*, 589–598.

Hummel, T., Vasconcelos, M.L., Clemens, J.C., Fishilevich, Y., Vosshall, L.B., and Zipursky, S.L. (2003). Axonal targeting of olfactory receptor neurons in Drosophila is controlled by Dscam. Neuron *37*, 221–231.

Jan, Y.N., and Jan, L.Y. (2003). The control of dendrite development. Neuron *40*, 229–242.

Kramer, A.P., and Kuwada, J.Y. (1983). Formation of the receptive fields of leech mechanosensory neurons during embryonic development. J. Neurosci. *3*, 2474–2486.

Kramer, A.P., and Stent, G.S. (1985). Developmental arborization of sensory neurons in the leech Haementeria ghilianii. II. Experimentally induced variations in the branching pattern. J. Neurosci. *5*, 768–775.

Lee, T., and Luo, L. (1999). Mosaic analysis with a repressible cell marker for studies of gene function in neuronal morphogenesis. Neuron *22*, 451–461.

Miller, F.D., and Kaplan, D.R. (2003). Signaling mechanisms underlying dendrite formation. Curr. Opin. Neurobiol. *13*, 391–398.

Montague, P.R., and Friedlander, M.J. (1991). Morphogenesis and territorial coverage by isolated mammalian retinal ganglion cells. J. Neurosci. *11*, 1440–1457.

Neves, G., Zucker, J., Daly, M., and Chess, A. (2004). Stochastic yet biased expression of multiple Dscam splice variants by individual cells. Nat. Genet. *36*, 240–246.

R Development Core Team. (2006). R: A Language and Environment for Statistical Computing. http://www.R-project.org.

Sagasti, A., Guido, M.R., Raible, D.W., and Schier, A.F. (2005). Repulsive interactions shape the morphologies and functional arrangement of zebrafish peripheral sensory arbors. Curr. Biol. *15*, 804–814.

Schmucker, D., Clemens, J.C., Shu, H., Worby, C.A., Xiao, J., Muda, M., Dixon, J.E., and Zipursky, S.L. (2000). Drosophila Dscam is an

axon guidance receptor exhibiting extraordinary molecular diversity. Cell *101*, 671–684.

Sdrulla, A.D., and Linden, D.J. (2006). Dynamic imaging of cerebellar Purkinje cells reveals a population of filopodia which cross-link dendrites during early postnatal development. Cerebellum *5*, 105–115.

Sugimura, K., Yamamoto, M., Niwa, R., Satoh, D., Goto, S., Taniguchi, M., Hayashi, S., and Uemura, T. (2003). Distinct developmental modes and lesion-induced reactions of dendrites of two classes of Drosophila sensory neurons. J. Neurosci. *23*, 3752–3760.

Sweeney, N.T., Li, W., and Gao, F.B. (2002). Genetic manipulation of single neurons *in vivo* reveals specific roles of Flamingo in neuronal morphogenesis. Dev. Biol. *247*, 76–88.

Wang, J., Zugates, C.T., Liang, I.H., Lee, C.H., and Lee, T. (2002). Drosophila Dscam is required for divergent segregation of sister branches and suppresses ectopic bifurcation of axons. Neuron *33*, 559–571.

Wang, J., Ma, X., Yang, J.S., Zheng, X., Zugates, C.T., Lee, C.H., and Lee, T. (2004a). Transmembrane/juxtamembrane domain-dependent Dscam distribution and function during mushroom body neuronal morphogenesis. Neuron *43*, 663–672.

Wang, Z., Singhvi, A., Kong, P., and Scott, K. (2004b). Taste representations in the Drosophila brain. Cell *117*, 981–991.

Whitford, K.L., Dijkhuizen, P., Polleux, F., and Ghosh, A. (2002). Molecular control of cortical dendrite development. Annu. Rev. Neurosci. *25*, 127–149.

Wojtowicz, W.M., Flanagan, J.J., Millard, S.S., Zipursky, S.L., and Clemens, J.C. (2004). Alternative splicing of Drosophila Dscam generates axon guidance receptors that exhibit isoform-specific homophilic binding. Cell *118*, 619–633.

Wong, A.M., Wang, J.W., and Axel, R. (2002). Spatial representation of the glomerular map in the Drosophila protocerebrum. Cell *109*, 229–241.

Zhan, X.L., Clemens, J.C., Neves, G., Hattori, D., Flanagan, J.J., Hummel, T., Vasconcelos, M.L., Chess, A., and Zipursky, S.L. (2004). Analysis of Dscam diversity in regulating axon guidance in Drosophila mushroom bodies. Neuron *43*, 673–686.

Zhu, H., Hummel, T., Clemens, J.C., Berdnik, D., Zipursky, S.L., and Luo, L. (2006). Dendritic patterning by Dscam and synaptic partner matching in the Drosophila antennal lobe. Nat. Neurosci. *9*, 349–355.

Zipursky, S.L., Wojtowicz, W.M., and Hattori, D. (2006). Got diversity? Wiring the fly brain with Dscam. Trends Biochem. Sci. *10*, 581–588.